ELSEVIER

Journal of Structural Geology 29 (2007) 467–480

JOURNAL OF STRUCTURAL GEOLOGY

www.elsevier.com/locate/jsg

Kinematic analysis of symmetrical natural folds developed in competent layers

Noel C. Toimil [a], F.J. Fernández [b,*]

[a] School of Earth, Ocean and Planetary Sciences, University of Cardiff, Cardiff CF10 3YE, UK
[b] Departamento de Geología, Universidad de Oviedo, Arias de Velasco s/n, Oviedo, Asturias 33005, Spain

Received 14 February 2006; received in revised form 6 October 2006; accepted 6 October 2006
Available online 21 November 2006

Abstract

Analysis of symmetrical folds developed in competent layers yields a kinematic folding model based on the study of the geometric characteristics of the folded layer, finite strain measurements and *c*-axis preferred orientation of detrital quartz. The meter-scale folds that we studied were formed during the first phase of Variscan deformation in the northwestern Iberian Massif. The strain sequence of the proposed model begins with initial layer shortening (ILSH) followed by tangential longitudinal strain (TLS), flexural flow (FF) and, finally, flattening (FL). In each fold, the intensity of each strain pattern has a small variation. FF is much less important than TLS and usually occurs after the latter due to the geometric incompatibilities developed during TLS. Neutral surface migration cannot completely explain the misfit between the strain measurements of the natural folds and the strain values predicted by the combination of the different strain patterns. This problem may be solved by considering a heterogeneous distribution of ILSH and FF, together with a modified tangential longitudinal strain. Heterogeneous area change across the fold profile could have also had an influence.

Keywords: Strain pattern; Folding; Strain measurement; Kinematics

1. Introduction

The final strain distribution within folded layers results from the accumulation of deformations affecting the layers. The study of the different strain patterns provides insight into the kinematic evolution of the folds from their initial undeformed stage to the final stage, which represents an essential basis for the restoration/balancing of structures.

The first studies for understanding strain patterns were by Kuenen and de Sitter (1938), Billings (1954, pp. 82–92), Ramberg (1961), Carey (1962), Donath (1962), Ramsay (1962), De Sitter (1964), Donath and Parker (1964) and Mukhopadhyay (1965). Subsequently, Ramsay (1967, pp. 391–436) analysed the kinematic models of tangential longitudinal strain (TLS), flexural flow (FF) and homogeneous deformation (HD). According to this author, for TLS the axes of the finite strain ellipses are arranged tangentially and perpendicularly to the layering. The layer is divided in two zones by a surface, known as the neutral surface, with no longitudinal strain (Fig. 1a). Strain magnitude increases with curvature and distance from the neutral surface. In this paper, we will use the term ''neutral line'', since the study has been made based on fold profiles (2D). FF is a layer-parallel simple shear, in which shear magnitude increases with greater layer dip change (Fig. 1b). HD, geometrically, represents an affine transformation of the layer points. It is called layer shortening if it occurs at the beginning of the folding, and flattening if it operates at the end (Fig. 1c,d). The geometrical effects on the folded layer are different in both cases. Ramsay and Huber (1987, pp. 445–473) studied the combination of FF with HD, and defined inverse tangential longitudinal strain as a deformation pattern characteristic of incompetent materials. Later, Bobillo-Ares et al. (2000) analysed TLS and the problems related to this

* Corresponding author.
E-mail address: brojos@geol.uniovi.es (F.J. Fernández).

0191-8141/$ - see front matter © 2006 Elsevier Ltd. All rights reserved.
doi:10.1016/j.jsg.2006.10.001

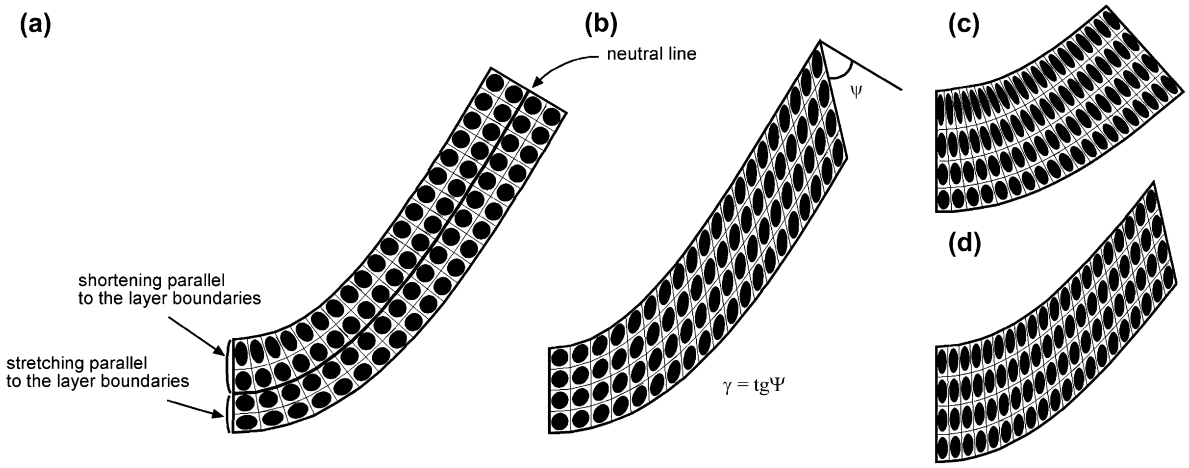

Fig. 1. Strain distribution of the different strain patterns on fold profiles. a) Pure tangential longitudinal strain; b) pure flexural flow (γ is shear strain); c) homogeneous deformation before buckling (initial layer shortening); and d) homogeneous deformation after buckling (flattening). In c) and d) the buckling stage is produce by tangential longitudinal strain.

strain pattern in detail. From the analysis of associated structures in the folds, secondary structures or strain in folds (i.e. Hudleston and Holst, 1984; Gutiérrez-Alonso and Gross, 1999; Ormand and Hudleston, 2003), an approximation to the strain patterns involved in the folding process has been obtained. Aspects such as the area decrease or the migration of the neutral line, which relate to strain accommodation during folding, have been treated by several authors (Gairola, 1978; Hudleston and Holst, 1984; Hudleston and Tabor, 1988; Ramsay and Huber, 1987, pp. 460–461; Hudleston and Lan, 1993; Lan and Hudleston, 1995, among others). Recently strain patterns have been modelled geometrically to investigate fold kinematic evolution (Bastida et al., 2003; Bobillo-Ares et al., 2004).

In this paper, we make a systematic and quantitative approximation to the different strain patterns: initial layer shortening (ILSH), TLS, FF and flattening (FL), responsible for the kinematic evolution in natural symmetric folds, for the case of competent layers. We analysed meter-scale folds developed during the first phase of the Variscan deformation in the northwestern Iberian Massif. We gathered geometric information about the shape of the folded surfaces, layer thicknesses, amplitudes, relationships between cleavage and layering, strain measurements, and *c*-axis preferred orientations of quartz. With these data, and using the computer program "*FoldModeler*" (Bobillo-Ares et al., 2004), we modelled the strain increment sequence and determined the relative importance of each strain pattern. Those factors that might have influenced the strain accommodation in certain zones of the folds, such as heterogeneous area change, neutral line migration and heterogeneous distribution of the strain patterns across the fold, are discussed.

2. Geological setting and characteristics of the folds

The analysed folds are located in the Cantabrian Zone (CZ), the West-Asturian Leonese Zone (WALZ) and the Centro-Iberian Zone (CIZ) of the northwest of the Iberian Massif (Lotze, 1945; Julivert et al., 1972) (Fig. 2). The Cantabrian Zone is characterized by the general lack of regional metamorphism and the presence of thin-skinned tectonics. The West-Asturian Leonese Zone is affected by greenschist facies regional metamorphism that generally increases westward, as does the deformation. The Centro-Iberian Zone is characterized by the abundance of granitoids and a metamorphism that, in general, is of higher grade than that of the WALZ. In the northwestern part of the Iberian Massif, three deformation phases can be distinguished during the Variscan orogeny (Matte, 1968; Marcos, 1973). The first phase produced kilometric scale folds with eastward vergence and associated minor folds. S_1 cleavage originated during this phase. The second deformation phase generated thrusts and shear zones, and the third phase produced a generalized crenulation and Ramsay's type III interference patterns.

Twenty-one folds of metric scale that formed during the first phase of Variscan deformation were analysed. They are located in four sectors: Lluanco – El Cabu Peñes (CZ), San Esteban – Cuideiru (WALZ), Tapia (WALZ) and La Cabrera (CIZ) (Fig. 2). From each sector, we gathered field data of folds developed in sandstone competent layers. In general, tectonic foliation S_1 is well developed in the four sectors, as slaty cleavage in pelitic levels and as spaced cleavage in sandstones and quartzites. For the present paper, we selected a collection of natural folds suitable for their treatment with *FoldModeler*, and which have to fulfil certain characteristics. Firstly, they must be approximately symmetric. In addition, the shape of the folded surface and layer and the relationships between layering and cleavage have to be measurable. Secondly, the folds selected must have developed in lithologies suitable for strain measurements.

All the folds analysed are developed in sandstones whose detrital grains are mainly formed by quartz, and to a lesser extent by feldspar (in some of the folds), with grain sizes ranging from very fine to medium sand (Fig. 3). Detrital grains are imbedded in a very fine matrix formed by small phyllosilicates (not visible to the naked eye) and microcrystalline quartz. Generally, rocks present a matrix-supported texture and develop

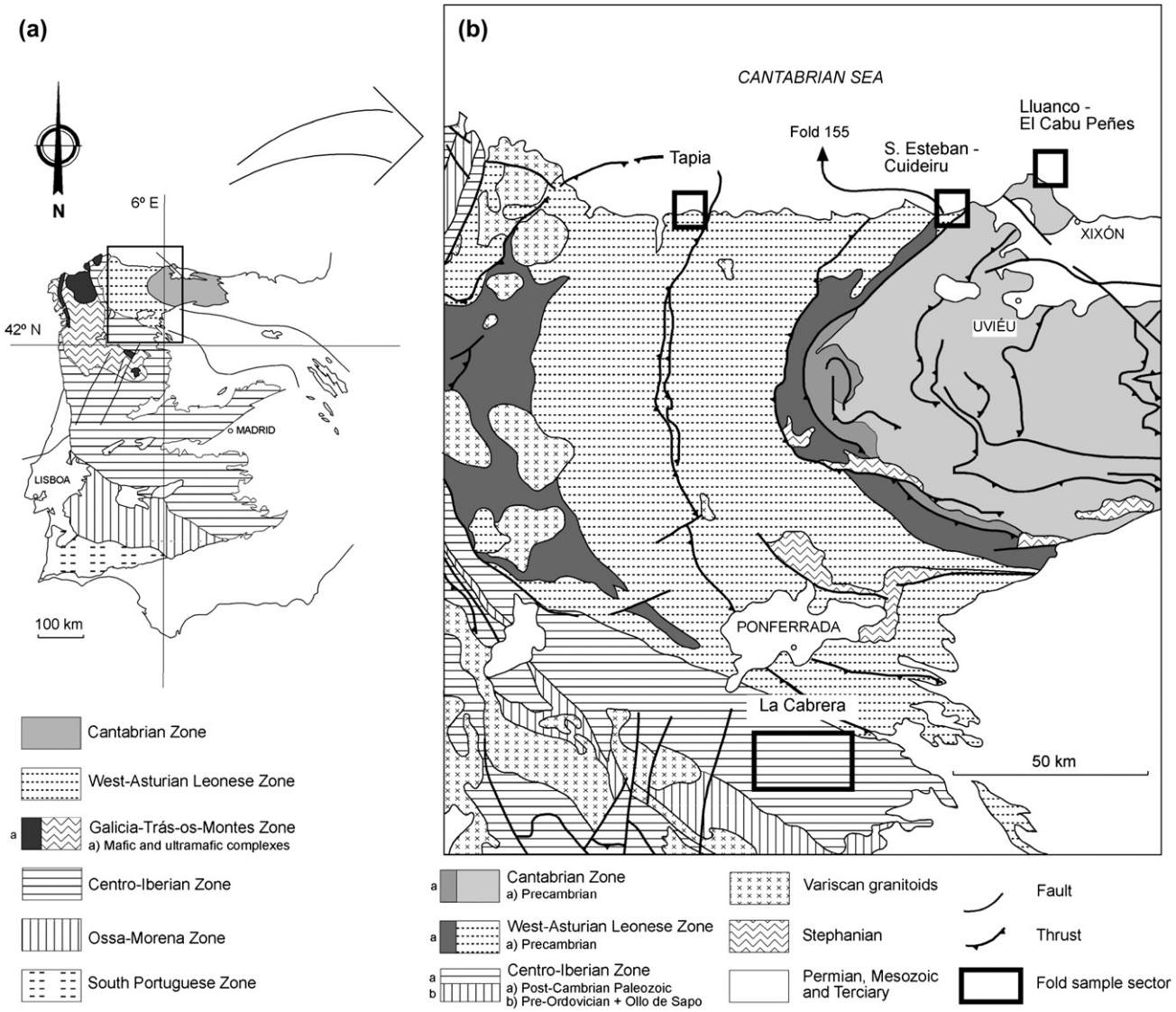

Fig. 2. Situation of the sectors where the analysed folds are located and situation of one of the folds that was analysed more in detail. a) Iberian Massif based on Julivert et al., 1972. b) NW of Iberian Massif based on Lotze (1945), Farias et al. (1987) y Martínez-Catalán et al. (1992).

rudimentary slaty cleavage. This microstructure is developed by intracrystalline plastic deformation (shown by elongated detrital grains and undulose extinction) and pressure solution (indicated by the presence of bands of insoluble material, irregular contacts among grains and beard structures). Cleavage is defined by matrix phyllosilicate orientation, detritic grain elongation and pressure solution bands.

3. Methodology

The computer program used to determine the strain pattern sequence responsible for strain accommodation in the folds analysed was *FoldModeler* (Bobillo-Ares et al., 2004). By the combination of TLS, FF and HD, this program makes it is possible to obtain theoretical folds whose geometric characteristics of surface and folded layer morphology, amplitude, strain distribution and intensity, are similar to those of the natural folds that are being analysed. Thus, it can be supposed that the sequence of strain patterns used to build the theoretical fold is similar to the sequence that has operated in nature to accommodate deformation in the natural fold. The study with *FoldModeler* is in 2D, on profiles of the folded layer (sections perpendicular to the fold axis), therefore, folds were treated as having a deformation history that involved plane straining. This is a simplification of the reality since there may be deformation along fold axis that is not taken into account. For the analysis, we start from an initial layer formed by a grid of quadrilaterals defined by points of known coordinates. On this grid, the strain patterns operate in a sequential manner modifying point positions according to geometric laws of each strain pattern. Once the sequence has been run, the final grid with the new positions of the quadrilaterals is obtained. The analysis of the final configuration allows us to find the geometric data of the folded layer, and by comparing the positions of the initial quadrilateral with their deformed positions, Cauchy's tensor can be calculated, from which the

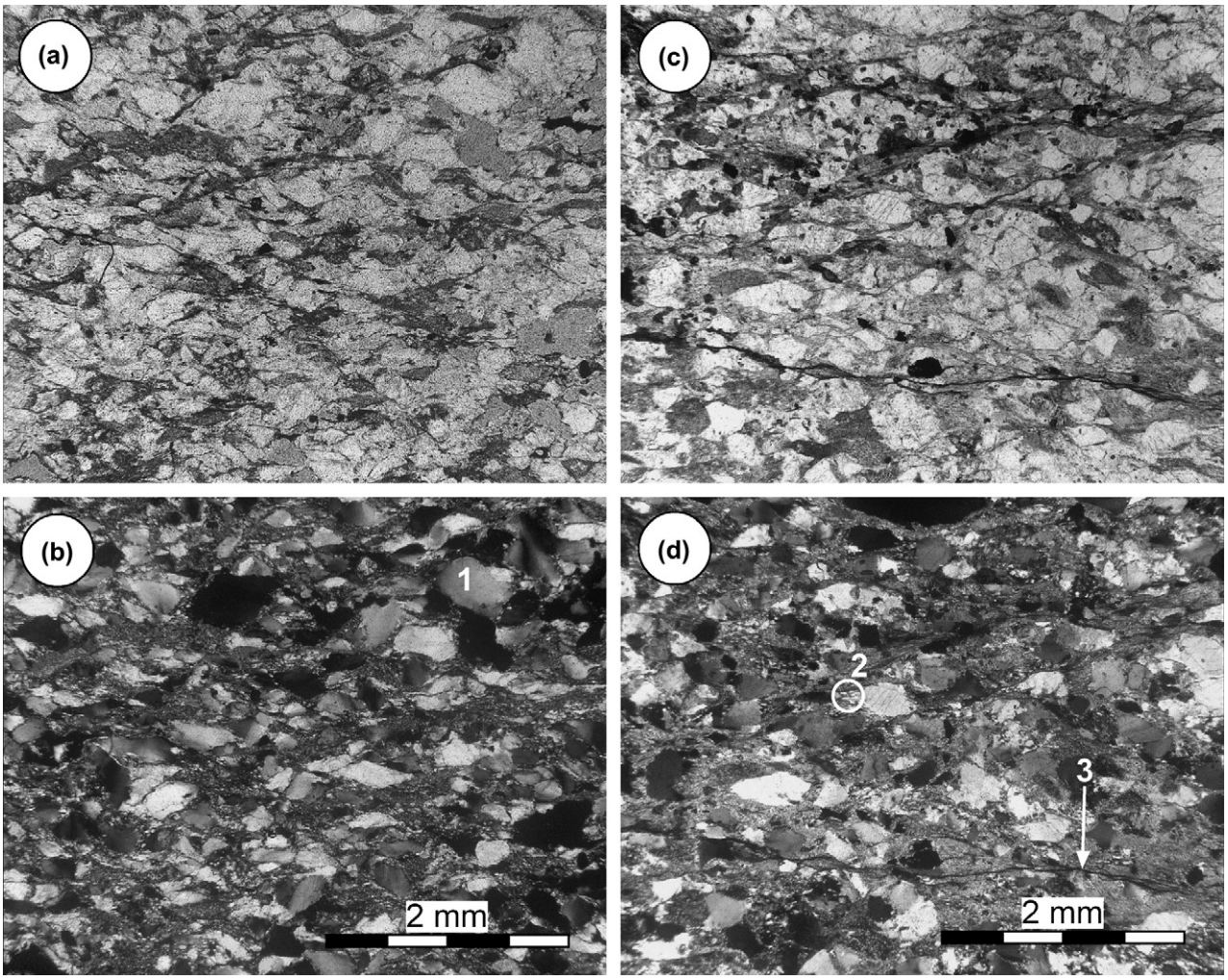

Fig. 3. Thin section photographs of a fold from San Esteban-Cuideiru sector. a) Inner arc, plane-polarized light; b) inner arc, crossed polars; c) outer arc, plane-polarized light; and d) outer arc, crossed polars. Cleavage is approximately parallel to the bottom of the photographs. Evidences of intracrystalline plastic deformation (undulose extinction) (1) and evidences of pressure solution (beard structures (2) and bands of insoluble material (3)) are indicated on the photographs.

principal finite strain values and directions are obtained for every point within the folded layer. Moreover, with *FoldModeler* it is also possible to simulate incremental neutral line migration (INL) (Ramsay and Huber, 1987, Fig. 21.21, Lan and Hudleston, 1995).

The establishment of the initial layer dimensions is necessary in order to estimate accurately the sequence of strain patterns. Depending on the initial thickness/length relationship of the layer, different amounts of ILSH must be applied to obtain the final geometry of the fold. The variation of ILSH implies a modification of the final R values (finite strain axial ratio). Given that we have strain data, we can determine the initial relation between thickness and length. This has been done following a trial and error process. That is to say, we modify the layer thickness and the amount of ILSH until we obtain the initial layer dimensions and ILSH value that, after folding, best match the final characteristics of the natural fold.

Once the initial layer is defined, sequences of strain patterns are run until one is found that best fits the data of the natural fold. The inputs are the different strain increments that form the sequence. Each increment is formed by one strain pattern (HD, TLS or FF). It is also necessary to specify the intensity of each strain pattern in each increment. To quantify the intensities of TLS and FF operating in the models, we used the variation of normalized amplitude (Δh) that the layer undergoes when the corresponding strain pattern takes place. In homogeneous deformation, the intensity has been measured as $|e_2|$; that is, as the absolute value of the extension (Ramsay and Huber, 1983, p. 281) measured in the direction of the short axis of the associated strain ellipse.

The basic outputs are (Fig. 4): a) geometry of folded surface, determined by a conic section (Aller et al., 2004), and its normalized amplitude ($h = y_0/x_0$); b) Ramsay's classification of the folded layer; c) variation in the inner and outer arc of the strain intensity with respect to layer dip (R-α); and d) variation in the orientation of the long axis of the finite strain ellipse (X) in the fold profile with respect to layer dip (ϕ-α).The outputs of the theoretical fold are compared with the geometric characteristics of natural fold to determine the goodness of the fit.

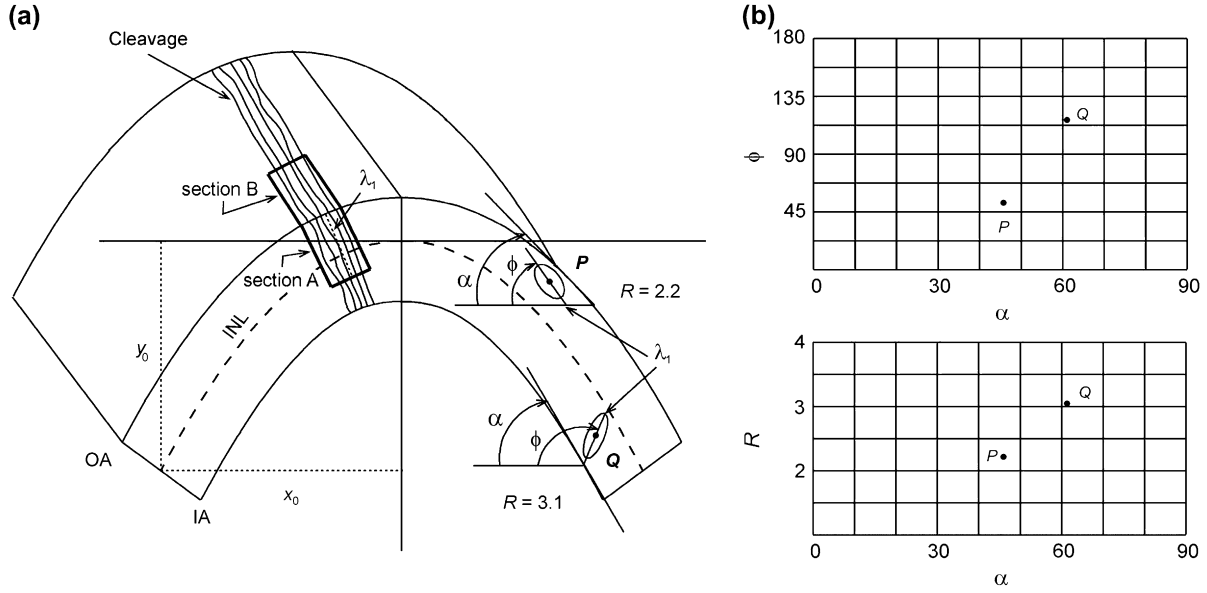

Fig. 4. a) Sections A and B of a fold and geometric meaning of normalized amplitude ($h = y_0/x_0$) and ϕ and α angles. Location of inner arc (IA), outer arc (OA) and incremental neutral line (INL). b) Diagrams of ϕ-α and R-α relationships.

To fit a fold, it is necessary to try (using a trial-and-error process) a large number of different combinations of the kinematic models until obtaining those sequences that best fit the data of the natural fold. The combinations differ in the different strain patterns involved in the sequence, in the intensity of each strain pattern, in the order of each one within the sequence, and in the number of times that they appear in the sequence. The process is repeated until reaching the sequences that best fit the data of the analysed fold. After that it is possible to constrain the strain patterns involved in the sequence, their order and intensities. In this paper, the whole process was repeated considering INL migration. This analysis yields predictions consistent with the measured finite strains and fold geometries. However, the lack of data related to the variation, with folding evolution, of strain values and their distribution within the layer, precludes that the models are uniquely correct. The same finite strain and geometry can result, in principle, from potentially a variety of deformation histories. However, the predictions are internally consistent for the sampled population of folded layers, and on that basis, we assume the predictions to be representative of the actual deformation histories.

Twenty-one folds profiles have been analysed in which at least four samples in each were taken to measure the strain: two in the hinge zone (inner and outer arc) and two in the limb (inner and outer arc). To do that, we have applied the "Delaunay Triangulation Nearest Neighbour Method (DTNNM)" (Mulchrone, 2002, 2005) on the quartz grains of the framework, measuring between 200 and 550 grains in each sample. In DTNNM, the nearest neighbours are determined by using Delaunay triangulation and the centre-to-centre distances are processed by normalisation (Erslev, 1988) and enhancement (Erslev and Ge, 1990) of the Fry method (Fry, 1979). The strain is estimated from the displacement of the grains after the deformation, and the final strain ellipse is calculated using a multiple linear least-squares regression method. In order to check and compare these results, we also used a shape marker method ($R_f-\phi$) (Ramsay, 1967, pp. 202–216) on the quartz grains of the framework, measuring once again between 200 and 550 grains in each sample. The calculation of the strain in this case was determined by fitting the data to the Θ-curves and the goodness of the fit was checked with the χ^2 method (Lisle, 1977; Lisle, 1985, pp. 15–17). The necessary parameters to use DTNNM and $R_f-\phi$ technique have been obtained with a GIS-Arcinfo V7.2.

Locally in folds where strain data are absent, strain geometry was approximated by assuming that the intersection of the cleavage plane with the fold profile is parallel to the orientation of the long semi-axis of the finite strain ellipse ($\sqrt{\lambda_1}$). In other words, we have supposed that the cleavage in every point of the layer is perpendicular to the shortening direction in that point.

In one of the folds of the San Esteban-Cuideiru sector (from now on fold 155) (Fig. 2b), deformation values in section B (perpendicular to cleavage and parallel to fold axis) have also been determined in order to obtain the 3D morphology of the strain ellipsoid. In this fold, we have also worked out the *c*-axis quartz fabrics in sections parallel to the fold profile (sections A) by optical means (U-stage) considering only the detrital grains of the framework, and excluding from the analysis the small grains of the matrix and microcrystalline quartz. We have studied the *c*-axis fabrics both to obtain an approximately 3D shape of the strain ellipsoid, and to detect possible asymmetries in the fabrics of the fold limbs, related to simple shear, and therefore to FF. The lack of more evidence of asymmetry in the texture has hampered the comparison of our results with those obtained by Williams and Jiang (1999) and Jiang (2001) who estimated the importance of different strain patterns by observing the rotation of porphyroblasts within the fold limb.

4. Results

Every fold was analysed and fitted using the methodology stated above. The sequences that fit the folds are different regarding the intensities of the different strain patterns involved, but it has been found that the order of the strain pattern is the same in all of them. Thus, we can define a standard sequence of the strain patterns that is the same for all the folds studied. This sequence starts with ILSH followed by TLS. Later deformation tends to be accommodated by FF and finally flattening (FL) takes place (Fig. 5). Moreover, for an individual fold, the intensities of each strain pattern involved in the fit present, in general, a small range of variation (Fig. 6). The smallest intensity variation for ILSH is 0.01, for TLS 0.04, for FF 0.04 and for FL 0.01. The largest variation for ILSH, TLS, FF and FL are respectively 0.1, 0.5, 0.42 and 0.11. No good fits were found outside the intervals shown in Fig. 6: 0.07–0.56 (ILSH), 0.2–1.50 (TLS), 0–1.12 (FF) and 0.02–0.40 (FL). On the other hand, we did not observe regional variations in the sequence of strain patterns or in their relative intensities.

All the folds need ILSH that can act simultaneously with TLS and/or FF. Good fits are obtained regardless of whether ILSH operates before TLS and/or FF or it takes place simultaneously with these two strain patterns. TLS is also essential in all the fits, whereas FF is only necessary in some cases and always to a lesser extent than TLS (Fig. 6). Generally, to reach good fits, FF must follow TLS. That is to say, although it is possible to have small intensities of FF before TLS, most of FF has to take place after TLS, which shows that as folding progresses there is a tendency for TLS to decrease and for FF to increase (Fig. 5). A homogeneous deformation stage (FL) at the end of folding is also necessary in all the cases. Most of the time, TLS simultaneous with FL is not possible, while FF is perfectly compatible with FL. Nevertheless, this simultaneity is usually incomplete; not all the FL can be applied together with the other strain patterns, but there is almost always a FL stage that acts alone at the end of the folding process.

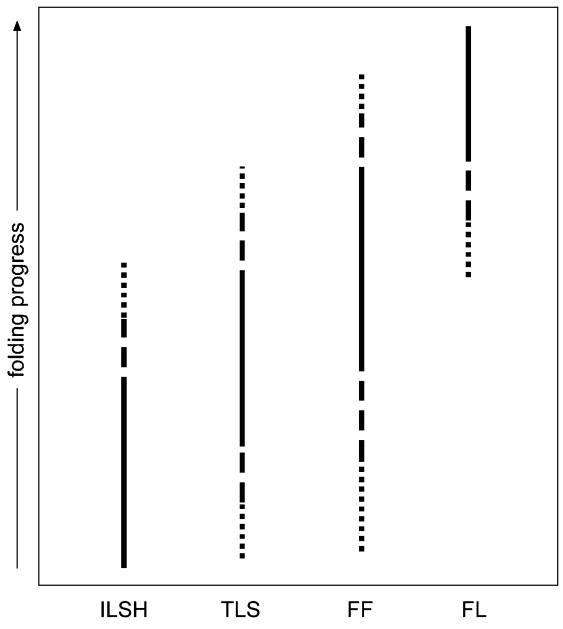

Fig. 5. Relationships between strain patterns and folding evolution. ILSH (initial layer shortening), TLS (tangential longitudinal strain), FF (flexural flow) and FL (flattening).

The strain values (R) obtained using DTNNM and R_f-ϕ technique are very similar. In DTNNM, to work out the R values, we have chosen the "selection factor" for each sample that minimized the error. The errors range between ± 0.1 (minimum) and ± 0.4 (maximum). Regarding the R_f-ϕ technique, the χ^2 method (applied to check the goodness of the Θ-curves fits) provides values always lower than 9, which means that the Θ-curves fit the data very well (Lisle, 1985, pp. 15–17).

In most of the folds $R < 2$ and there are no strong differences from the inner to the outer arc, or from the hinge to the limbs (Figs. 7 and 8). In general, there are no sequences in which, by combining the strain patterns considered in this paper, it is possible to fit all the fold data and at the same time to obtain strain values similar to those determined by DTNNM or R_f-ϕ method. Theoretical R-α relationships given by *FoldModeler* show a variation from the limbs to the hinge, and from the outer to the inner arc. Additionally, R values, especially in the inner arc, are much larger than natural values. This happens even taking into account the fact that to define the initial layer in each fold, we selected the layer whose initial proportions had the largest thickness/length relationship possible in each case. That is to say, we selected the one that needed the least amount of ILSH, and that therefore provided the minimum values of finite strain. The fit with INL migration (Figs. 7 and 8) gives lower R values in the hinge zone, coming a little closer to the strain values calculated, but in most cases it yields a worse Ramsay's classification and a worse fit of the ϕ-α curves (Fig. 7).

The sequence of strain pattern obtained with *FoldModeler* does not imply area change within the fold. We estimated the area decrease that would be necessary to match the strain values of the natural folds with those obtained theoretically (Fig. 9). In each quadrilateral of the theoretical fold developed with *FoldModeler* there is a strain ellipse, where R, $\sqrt{\lambda_1}$ and $\sqrt{\lambda_2}$ are known. We supposed that the semi-axis $\sqrt{\lambda_2}$ in that quadrilateral has the same value as the equivalent zone in the natural fold. Therefore, it is possible to know the area decrease (Δ) in this zone of the natural fold: $\Delta = \sqrt{\lambda_1}\sqrt{\lambda_2}$, where $\sqrt{\lambda_2}$ is known, since it is considered to be the same as in *FoldModeler*, and $\sqrt{\lambda_1} = R_m\sqrt{\lambda_2}$, R_m being the mean value of the finite strain obtained with DTNNM and R_f-ϕ technique. We obtained a mean value of area decrease for all the folds in the inner arc of 65% and in the outer arc of 26%. This way of accommodating the deformation is comparable to the "inner arc collapse" described by Hudleston and Holst (1984).

In order to understand the 3D strain and the deformation regime within the folded layer, we measured the R values of sections A and B in fold 155 (Figs. 10 and 11), and we observed that the relationships between the axes of finite strain in the two sections were very similar. The ellipsoid in every point sampled was plotted in a Flinn diagram (Fig. 12). All the points lie within the field of flattening ellipsoids in the case

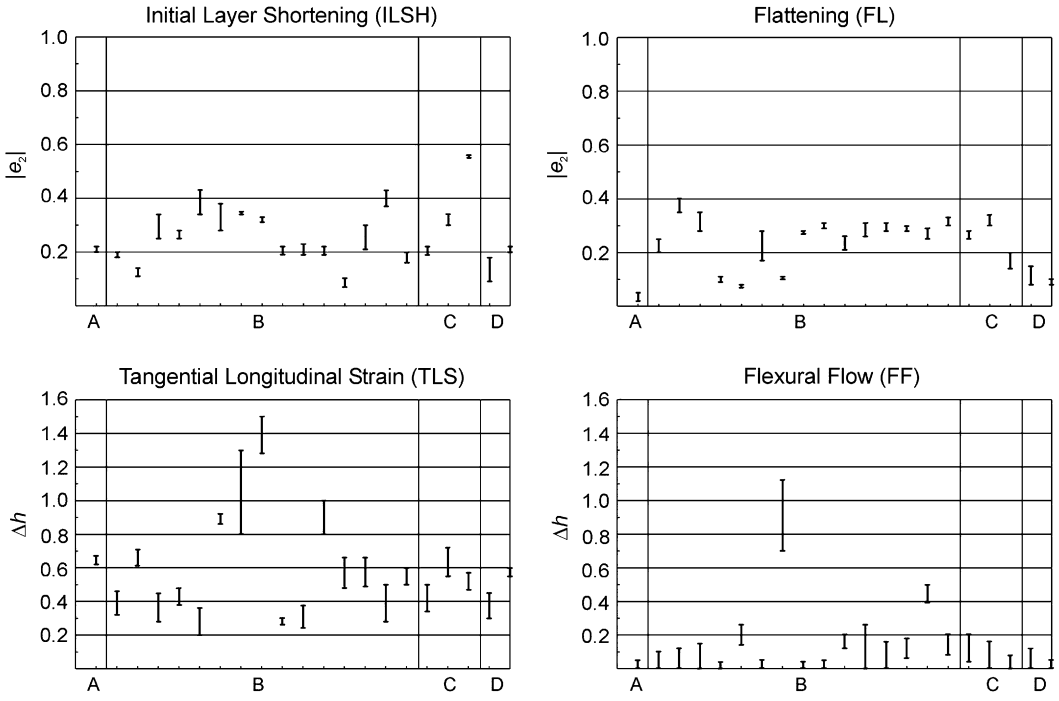

Fig. 6. Intensity variation range of the different strain patterns in all the analysed folds. ILSH and FL intensities are measured as $|e_2|$ and TLS and FF intensities as Δh (see text). A (Lluanco-El Cabu Peñes sector), B (San Esteban-Cuideiru sector), C (Tapia sector) and D (La Cabrera sector).

of no volume change, and most of them are located close to the origin of the coordinates, below the limit of the necessary deformation for cleavage development according to Ramsay and Wood (1973) and Wood (1974). The calculated ellipsoids have X/Y and Y/Z relationships lower than the results obtained by other authors in slates with cleavage that formed in greenschist facies metamorphic conditions similar to those of the analysed folds. The existence of deformation along the fold axis indicates that there is certain amount of strain which cannot be detected by studying folds with *FoldModeler*, since this program analyse profiles of folds.

Quartz fabrics along the fold shows a *c*-axis pattern characterized by a symmetric cross girdle normal to *b* with a large half opening angle (Fig. 10). This corresponds to a constrictive regime (e.g., Lister and Hobbs, 1980) and shows stretching parallel to the fold axis. It is difficult to explain the inconsistence between the ellipsoid obtained using strain data and the one using *c*-axis. The study of the thin sections of the samples did not provide any evidence that indicated that the stretching in *b* direction is substantially larger than in *a*. If there was no volume change, according to the strain data, there would be stretching parallel to the fold axis (*b* direction) as well as perpendicular to it (*a* direction). On the other hand, the symmetrical pattern of the fabric suggests that FF was not operative, which agrees with the results of the fits achieved with *FoldModeler* (Fig. 7c).

5. Discussion

The model of strain pattern sequence by which the analysed folds accommodate deformation is similar in all of them. However, the relative intensity of the strain patterns varies depending on the different bulk shortening produced, the mechanical properties of the layer, and the specific characteristics of the multilayer where the fold is located. On the other hand, we found that the largest intensity of FF must take place after TLS. This is due to the geometric incompatibilities of the later strain pattern, since when the fold presents a marked amplification with high curvature in the hinge zone (advanced folding stages), strain accommodation by TLS produces high deformations in this zone, especially in the inner arc. These large strain values are not observed in the studied folds.

Homogeneous deformation can act simultaneously with TLS and/or FF, either at the beginning of folding evolution (ILSH) or at the end (FL). It is difficult to guess with the methodology used in this paper whether this simultaneity occurs or not, since both cases provide good fits of the data. In the case of ILSH, buckling theory states that this strain pattern takes place simultaneously with TLS and/or FF, and that these two strain patterns increase their importance as the fold progresses (i.e., Ramberg, 1964). Regarding FL, usually simultaneous combination of FL with TLS is impossible since in advanced stages of folding evolution, the fold is usually fairly amplified and shows a relatively high curvature in the hinge zone, causing large deformations in the inner arc of this area that do not agree with strain measurements. In contrast, FF does not present this geometric incompatibility, and therefore it can operate simultaneously with FL, which explains why FF increases its importance with respect to TLS as folding progresses. However, FF cannot combine completely with FL. A single FL stage at the end of folding is almost always required to reach a good fit of the data, which can be due to that, from a mechanical point

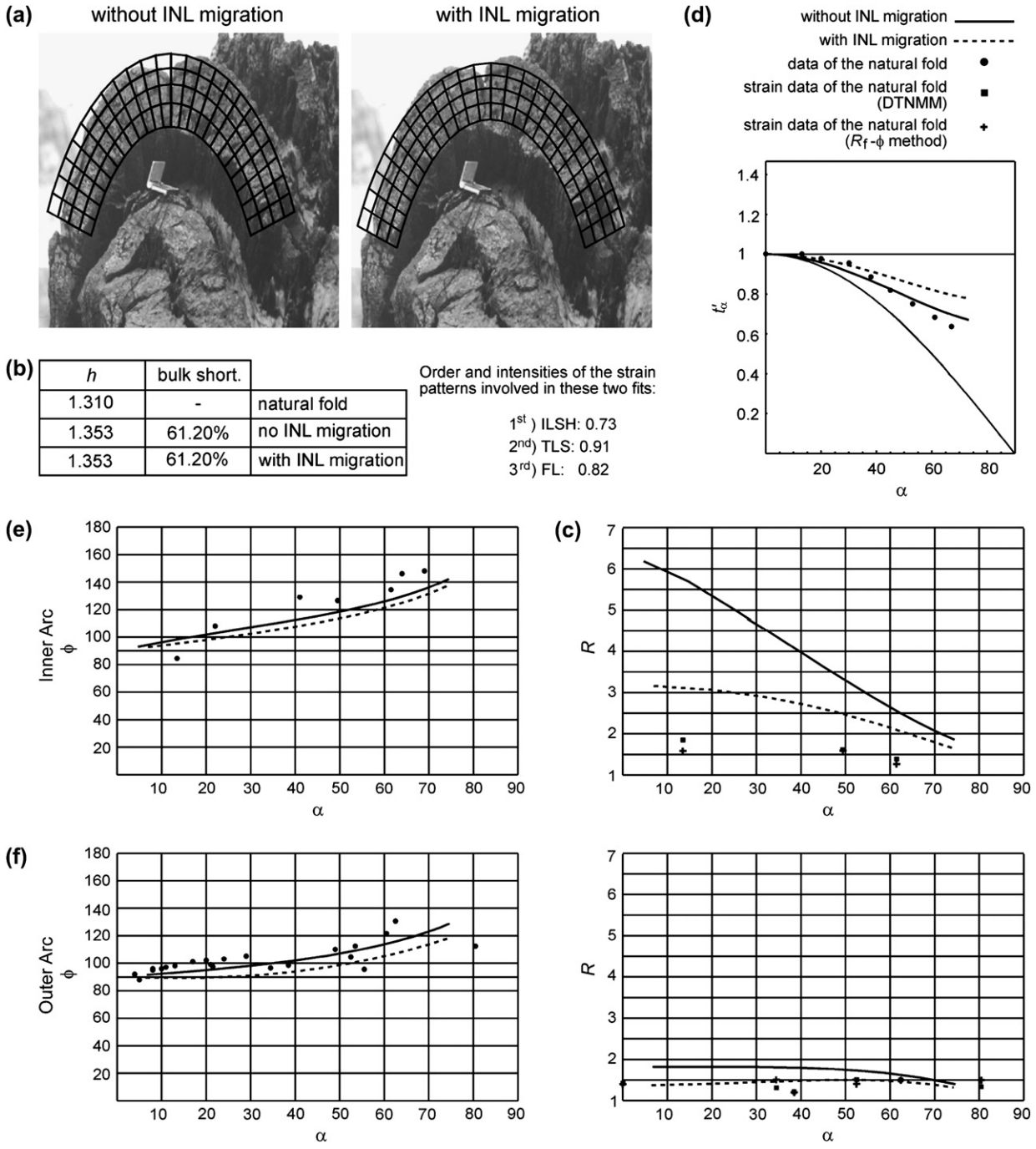

Fig. 7. Results of two fits carried out on fold 155, with and without INL migration. a) Natural fold with two superimposed theoretical folds obtained with *Fold-Modeler*. b) Comparison between real *h* and theoretical *h*. c) Sequence of strain patterns. d) Fit of the Ramsay's classification. e) Fit of the ϕ-θ and *R*-α relationships in the inner arc and f) Fit of the ϕ-θ and *R*-α relationships in the outer arc.

of view, in marked 1C folds, simple shear parallel to layer boundaries is hampered, since these limits are not parallel. These results suggest that in final stages of folding evolution, pure FL becomes progressively more important with respect to the other strain patterns that can take place simultaneously with it. Therefore, this interpretation constitutes an intermediate situation between pure flattening in advance stages of folding (Ramsay, 1962, 1967, pp. 411–415), and simultaneity between buckling and flattening (Hudleston, 1973).

The misfit of the strain data (*R*), especially in the inner arc, was the main problem found in the analysis of natural folds. In principle, this fact can be explained by different causes:

5.1. Migration of incremental neutral line (INL)

The displacement of the INL towards the inner arc during folding could decrease the strain enough in this zone to solve the problem. However, in the cases under study here, the

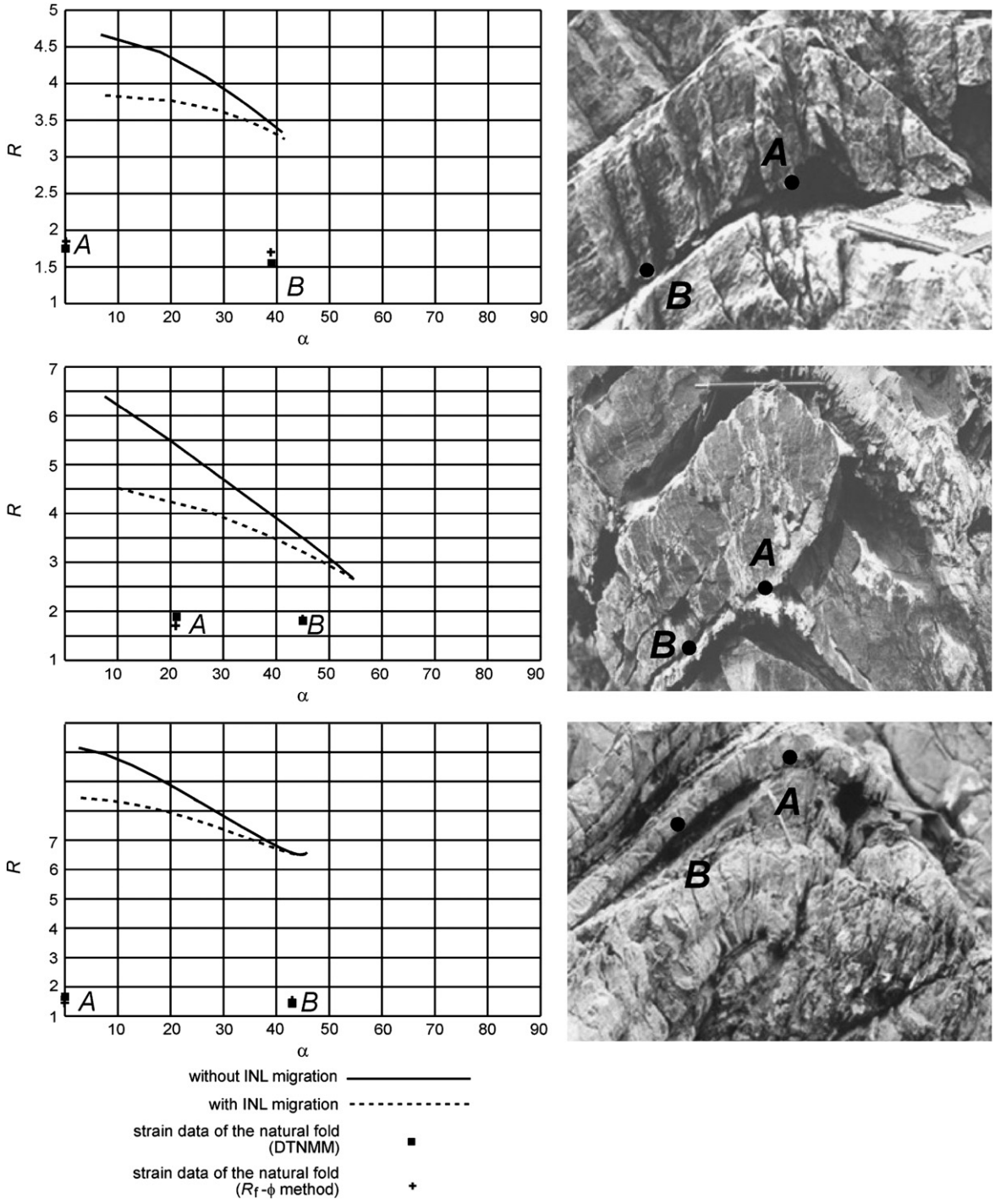

Fig. 8. Misfit of the R data in the inner arcs of three analysed folds. Results obtained with and without INL migration.

migration of the INL did not give good fits for the R-ϕ curves and for other geometric parameters of the fold (Figs. 7 and 8), although it did reduce the differences between the R values of the natural folds and the theoretical values given by the program.

5.2. The methods used to calculate R are not suitable

The R values stated in this paper must reflect quite accurate the real bulk strain that the rocks underwent, since using different methods we have reached approximately the same results. However, under several conditions these methods can underestimate the strain. Fig. 12 might represent an indication in this regard, because all the values obtained are lower than the results reached by other authors. In the DTNNM, underestimation of strain may happen when the original grain distribution is not anticluster and random, while in R_f-ϕ method it occurs when all the strain does not result in a change of the grain shape. Besides, it is also possible that deformation

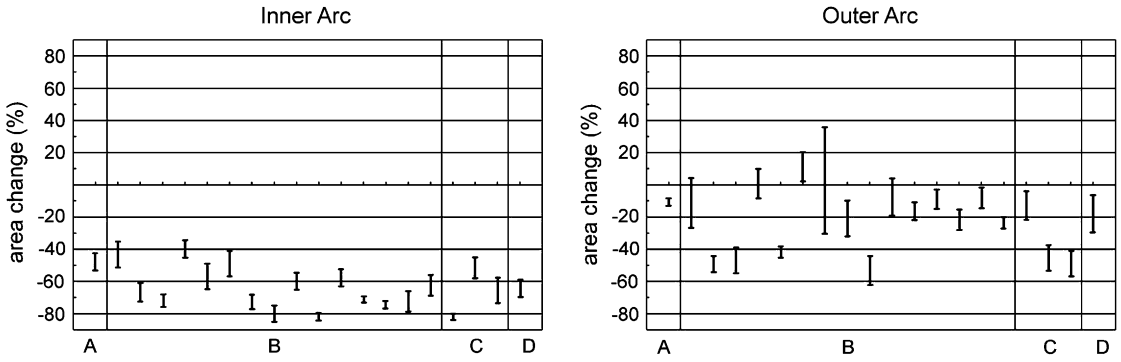

Fig. 9. Area variation on the fold profile that is necessary to fit the *R* strain values in the inner and the outer arcs of the analysed fold. A (Lluanco-El Cabu Peñes sector), B (San Esteban-Cuideiru sector), C (Tapia sector) and D (La Cabrera sector).

mechanisms such as grain-boundary sliding occur, which is very difficult to detect in detrital textures such as those studied in this paper (Narahara and Wiltschko, 1986).

5.3. Heterogeneous area change

If we suppose that the values obtained by the application of the methods used are approximately correct, another possibility to explain the misfit is that there is a heterogeneous area change. The result would be an area decrease in the inner arc, generating less deformation than expected. If this is the case, an average area decrease of 65% in the inner arc and 26% in the outer arc would be necessary. These data, although a little higher in the inner arc, are not very different from those obtained from the analysis of folded quartz veins by Druguet and Griera (1998), who gave values of area decrease of between 30 and 50%. In the analysed natural folds there is evidence of pressure solution associated with cleavage development. Area change can, therefore, be possible, although apparently there is nothing that indicates a larger decrease in the inner arc than in the outer one, since the two arcs show the same microstructural characteristics (Fig. 3). Huldeston and Tabor (1988) studied the strain accommodation in a buckled calcite vein and found that all the features observed matched a sequence of ILSH + TLS together with an area decrease in the inner arc originated by pressure solution.

5.4. Variation of the strain pattern intensities across the layer

If the calculated strain values are close to real ones, another possibility is that the deformation is not accommodated according to the strain patterns considered in *FoldModeler*. Toimil (2005), studying experimental and numerical folds, observed strain problems similar to those found in this paper. They solved them by considering that ILSH and FF have a variable intensity across the layer, the former presenting a slightly variation, while FF is much more intense in the central parts of the layer than near the boundaries. The deformation produced by TLS is less intense than was established for this strain pattern in the classical model, which results in less shortening parallel to the layer in the inner arc and less stretching in the outer arc. However, this possibility could not be checked reliably in the natural folds analysed, since in order to do that it would have been necessary to define multiple rows within the folded layer so as to determine very precise geometric and strain data. This task is very difficult in the study of natural folds.

6. Conclusions

The geometric analysis carried out on metric scale symmetric folds developed in competent layers during the first phase of the Variscan deformation of the northwest of the Iberian Massif has enabled the definition of a kinematic model for the evolution of these folds, which is consistent with earlier work. Thus, we have obtained a standard sequence of strain patterns, valid for all the folds, formed by an ILSH stage, followed by TLS, subsequently FF (not always), and finally FL. The geometric methodology is therefore a suitable way of knowing the evolution of the folds. Although the sequence is the same in all the folds analysed, in each one the intensity of the strain patterns that take part is different, which is related to the different mechanical properties of the layers, the bulk shortening undergone and the characteristics of the multilayer.

The fact that TLS is much more important than FF in the middle stages of folding may be due to the fact that in single competent layers low anisotropy is expected. When these two strain patterns operate in a fold, the deformation tends to be accommodated first by TLS and then by FF, owing to the geometric incompatibilities of the former. Therefore, FF intensity increases, in general, as the folding progresses.

Regarding the homogeneous deformation, ILSH can take place as a single stage or combined with TLS and/or FF, while FL, even though it can operate simultaneously with TLS and/or FF, generally takes place alone in the most advanced stages of folding evolution.

The low intensity of the strain cannot be completely explained only with the traditional strain patterns stated above. The finite strain data obtained with DTNNM and R_f-ϕ technique are much lower, especially in the inner arc of the folds, than the theoretical values expected. This might be explained by considering a heterogeneous distribution of ILSH and FF, together with a modified model of TLS. Nevertheless, area decrease in the inner arc and INL migration could have also been

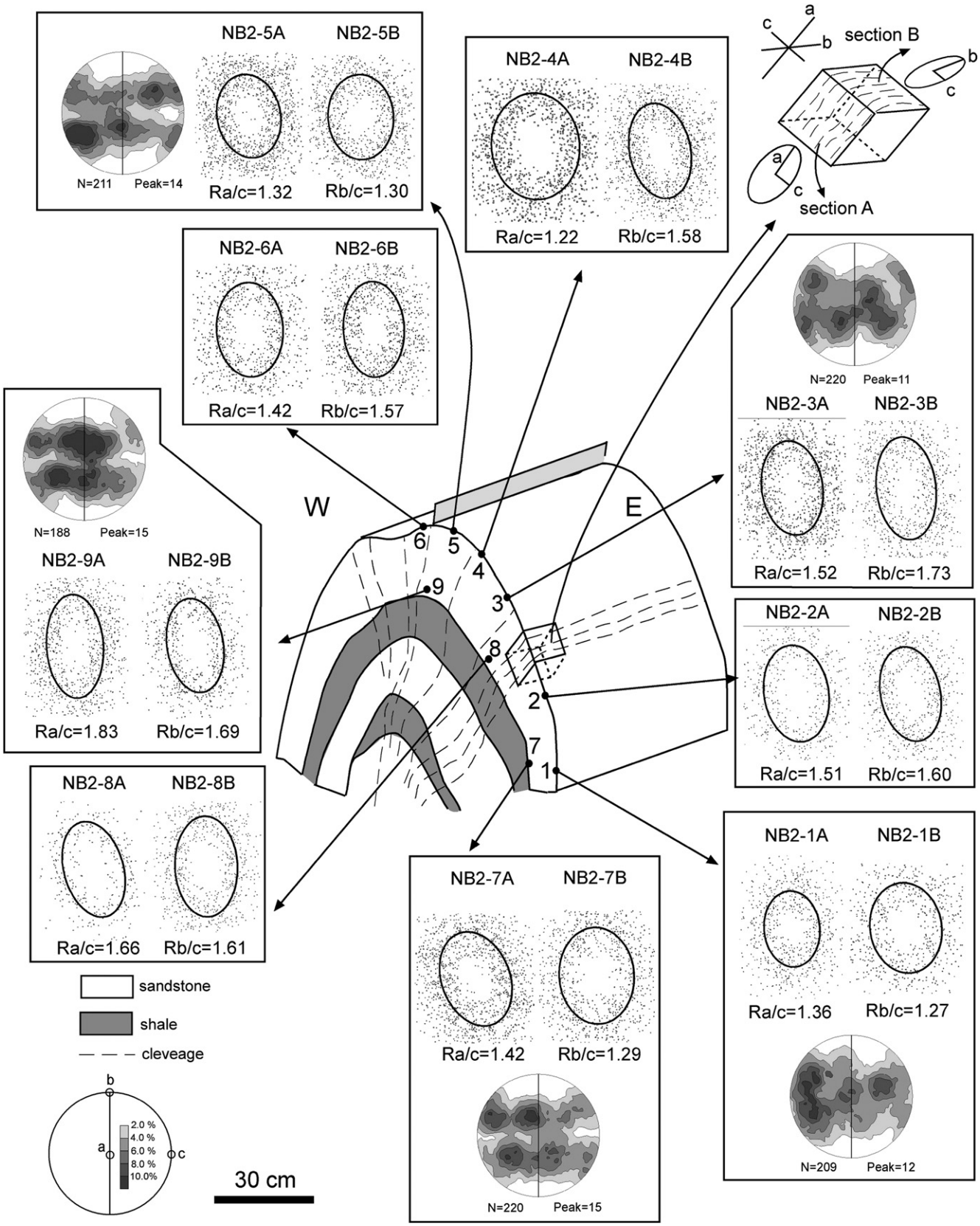

Fig. 10. Strain values achieved with the DTNNM in two perpendicular sections of the fold 155, and *c*-axis preferred orientation of quartz grains (equal area projection, lower hemisphere).

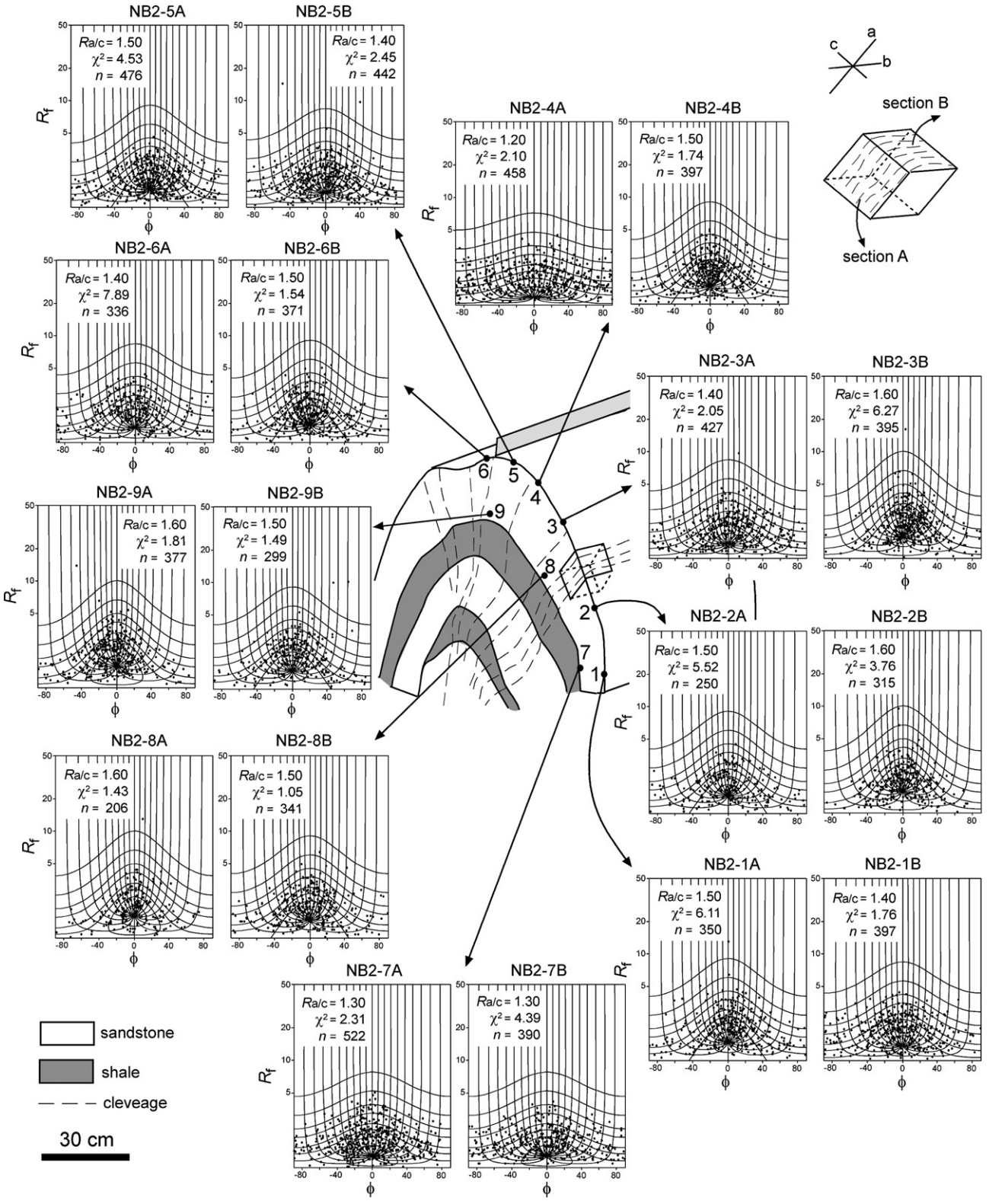

Fig. 11. Strain values achieved with the R_f-ϕ technique in two perpendicular sections of the fold 155. Values of χ^2 and number of data (n) used are also indicated.

of importance. Deformation mechanisms such as grain-boundary sliding can produce an underestimation in the measured finite strain, which would generate strain values closer to those theoretically expected.

Acknowledgements

The present paper has been supported by Spanish BTE2002-00187 project funded by Ministerio de Educación

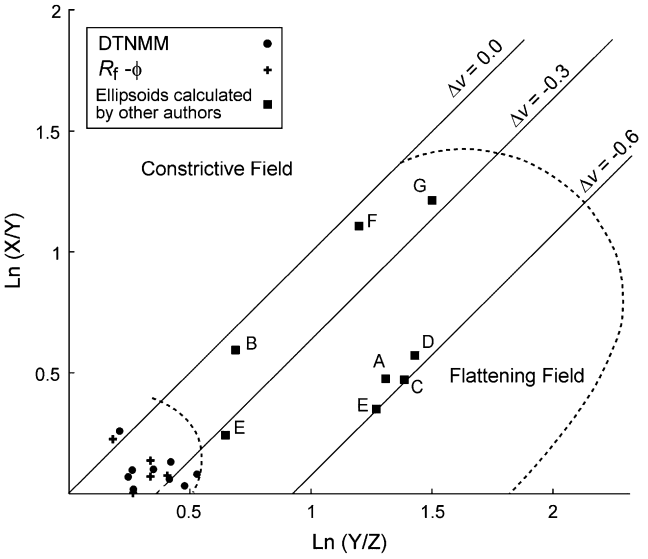

Fig. 12. Flinn diagram with the R values obtained with DTNNM and the R_f-ϕ technique in fold 155. Plane strain line for different values of volumetric change (Δv) and mean strain ellipsoids for cleavaged rocks from different authors are plotted: A (Sorby, 1853), B (Hill and Thomas, 1944), C (Ramsay and Wood, 1973), D (Wood, 1974), E (Beutner and Charles, 1985), F (Gray and Willman, 1991) y G (Tan et al., 1995). Dashed lines indicate the lower and upper limits for cleavage formation according to Ramsay and Wood (1973) and Wood (1974).

y Ciencia and a postdoctoral grant awarded by Secretaría de Estado de Universidades e Investigación del Ministerio de Educación y Ciencia. We are grateful to the reviewers Peter Hudleston, Dyanna Czech and the editor Bill Dunne whose critical comments have resulted in a greatly improved manuscript. We also thank Jesús Aller for many valuable suggestions, Richard Lisle for his advice on the R_f-ϕ technique, Kieran Mulchrone for providing us with his program, Rosana Menéndez for helping us with the GIS and Robin Walker for his revision of the English.

References

Aller, J., Bastida, F., Toimil, N.C., Bobillo-Ares, N.C., 2004. The use of conic sections for the geometrical analysis of folded surface profiles. Tectonophysics 397, 239–254.

Bastida, F., Bobillo-Ares, N.C., Aller, J., Toimil, N.C., 2003. Analysis of folding by superposition of strain patterns. Journal of Structural Geology 25, 1121–1139.

Beutner, E.C., Charles, E.G., 1985. Large volume loss during cleavage formation, Hamburg sequence, Pennsylvania. Geology 13, 803–805.

Billings, M.P., 1954. Structural Geology, second ed. Prentice Hall, Englewood Cliffs, New Jersey, 514 pp.

Bobillo-Ares, N.C., Bastida, F., Aller, J., 2000. On tangencial longitudinal strain folding. Tectonophysics 319, 53–68.

Bobillo-Ares, N.C., Toimil, N.C., Aller, J., Bastida, F., 2004. 'FoldModeler': a tool for the geometrical and kinematical analysis of folds. Computers and Geosciences 30, 147–159.

Carey, S.W., 1962. Folding. Journal of the Alberta Society of Petroleum Geologists 10, 95–144.

De Sitter, L.U., 1964. Structural Geology, 2nd Edition. McGraw-Hill, New York, 551 pp.

Donath, F.A., 1962. Role of layering in geologic deformation. Transactions of the New York Academy of Sciences 24, 236–249.

Donath, F.A., Parker, R.B., 1964. Folds and folding. Geological Society of American Bulletin 75, 45–62.

Druguet, E., Griera, A., 1998. Strain analysis using deformed quartz veins. Geogaceta 24, 119–122.

Erslev, E.A., 1988. Normalized centre-to-centre strain analysis of packed aggregates. Journal of Structural Geology 10, 201–209.

Erslev, E.A., Ge, H., 1990. Least squares centre-to-centre and mean object ellipse fabric analysis. Journal of Structural Geology 8, 1047–1059.

Farias, P., Gallastegui, G., González Lodeiro, F., Marquínez, J., Martín-Parra, L.M., Martínez Catalán, J.R., Pablo Maciá, J.G., Rodríguez-Fernández, L.R., 1987. Aportaciones al conocimiento de la litoestratigrafía y estructura de Galicia Central. Memmórias do Museo e laboratorio Mineralógico e Geológico, Facultade de Ciências, Universty of Porto 1, 411–431.

Fry, N., 1979. Random point distributions and strain measurement in rocks. Tectonophysics 60, 89–105.

Gairola, V.K., 1978. Strain distribution across an experimental single-layer fold. Tectonophysics 44, 27–40.

Gray, D.R., Willman, C.E., 1991. Thrust-related strain gradients and thrusting mechanisms in a chevron-folded sequence, southeastern Australia. Journal of Structural Geology 13, 691–710.

Gutiérrez-Alonso, G., Gross, M.R., 1999. Structures and mechanisms associated with development of a fold in the Cantabrian Zone thrust belt, NW Spain. Journal of Structural Geology 21, 653–670.

Hill, E.S., Thomas, D.E., 1944. Deformation of graptolites. Geological Magazine 81, 216–222.

Hudleston, P.J., 1973. Fold morphology and some geometrical implications of theories of fold development. Tectonophysics 16, 1–46.

Hudleston, P.J., Holst, T.B., 1984. Strain analysis and fold shape in a limestone layer and implications for layer rheology. Tectonophysics 106, 321–347.

Hudleston, P.J., Lan, L., 1993. Information from fold shapes. Journal of Structural Geology 15, 253–264.

Hudleston, P. J., Tabor, S. H., 1988. Strain and fabric development in a buckled calcite vein and rheological implication. Bulletin of the Geological Institutions of the University of Uppsala, N.S. 14, 79–94.

Jiang, D., 2001. Reading history of folding from porphyroblasts. Journal of Structural Geology 23, 1327–1335.

Julivert, M., Fontboté, J.M., Ribeiro, A., Conde, L., 1972. Mapa tectónico de la Península Ibérica y Baleares. Instituto Geológico y Minero de España, 113 pp.

Kuenen, P.H., de Sitter, L.U., 1938. Experimental investigation into the mechanisms of folding. Leidsche Geologische Mededelingen 60, 217–240.

Lan, L., Hudleston, P.J., 1995. The effects of rheology on the strain distribution in single layer buckle folds. Journal of Structural Geology 17, 727–738.

Lisle, R.J., 1977. Clastic grain hape and orientation in relation to cleavage from the Aberystwyth Grits, Wales. Tectonophysics 39, 381–395.

Lisle, R.J., 1985. Geological Strain Analysis, A Manual for the R_f-ϕ Technique. Pergamon Press, Oxford, 99 pp.

Lister, G.S., Hobbs, B.E., 1980. The simulation of fabric development during plastic deformation and its application to quartzite: the influence of deformation history. Journal of Structural Geology 2, 355–370.

Lotze, F., 1945. Zur Gliderung der Varisziden der Iberischen Meseta. Geotektonische Forschungen 6, 78–92.

Marcos, A., 1973. Las series del Paleozoico inferior y la estructura herciniana del occidente de Asturias (NW de España). Trabajos de Geología 6, 1–113.

Martínez-Catalán, J.R., Rodríguez, M.P.H., Alonso, P.V., Pérez-Estaún, A., González-Lodeiro, F.G., 1992. Lower Paleozoic extensional tectonics in the limit between the West Asturian-Leonese and Central Iberian Zones of the Variscan fold-belt in NW Spain. Geologische Rundschau 81, 545–560.

Matte, P., 1968. La structure de la virgation hercynienne de Galice (Espagne). Revue Geologie Alpine 44, 1–128.

Mukhopadhyay, D., 1965. Effects of compression on concentric folds and mechanism of similar folding. Journal of the Geological Society of India 6, 27–41.

Mulchrone, K.F., 2002. Application of Delaunay triangulation to the nearest neighbour method of strain analysis. Journal of Structural Geology 25, 689–702.

Mulchrone, K.F., 2005. DTNNM: A windows program for strain analysis using the Delaunay triangulation nearest neighbour method. Computers and Geosciences 31, 978–988.

Narahara, D.K., Wiltschko, D.V., 1986. Deformation in the finge region of a chevron Fol., Valley and Ridge Province, central Pennsylvania. Journal of Structural Geology 8, 157–158.

Ormand, C.J., Hudleston, P.J., 2003. Strain paths of three small folds from the appalachian Valley and Ridge, Maryland. Journal of Structural Geology 25, 1841–1854.

Ramberg, H., 1961. Relationship between concentric longitudinal strain and concentric shearing strain during folding of homogeneous sheets of rocks. American Journal of Science 259, 382–390.

Ramberg, H., 1964. Selective buckling of composite layers with contrasted rheological properties: a theory for simultaneous formation of several orders of folds. Tectonophysics 6, 307–341.

Ramsay, J.G., 1962. The geometry and mechanics of 'similar' type folds. Journal of Structural Geology 70, 309–327.

Ramsay, J.G., 1967. Folding and Fracturing of Rocks. McGraw-Hill, New York, 568 pp.

Ramsay, J.G., Huber, M.I., 1983. The Techniques of Modern Structural Geology. In: Strain Analysis, vol. 1. Academic Press, London, pp. 1–308.

Ramsay, J.G., Huber, M.I., 1987. The Techniques of Modern Structural Geology. In: Folds and Fractures, vol. 2. Academic Press, London. pp. 309–700.

Ramsay, J.G., Wood, D.S., 1973. The geometric effects of volume change during deformation processes. Tectonophysics 16, 263–277.

Sorby, H.C., 1853. On the origin of slaty cleavage. New Philosophical Journal 55, 137–148.

Tan, B.K., Gray, D.R., Stewart, I., 1995. Volume change accompanying cleavage development in graptolitic shales from Gisborne, Victoria, Australia. Journal of Structural Geology 17, 1387–1394.

Toimil, N.C., 2005. Geometría y patrones de deformación de pliegues simétricos desarrollados en capas competentes. Ph.D. thesis, University of Oviedo, Oviedo, 270 pp.

Williams, P.F., Jiang, D., 1999. Rotating garnets. Journal of Metamorphic Geology 17, 367–378.

Wood, D.S., 1974. Current views on the development of slaty cleavage. Annual Review of Earth and Planetary Sciences 2, 369–401.